Atmos. Chem. Phys. Discuss., 15, 13173–13209, 2015
www.atmos-chem-phys-discuss.net/15/13173/2015/
doi:10.5194/acpd-15-13173-2015

Atmospheric Chemistry and Physics Discussions

Vertical variations of aerosols and the effects responded to the emission control: application of lidar ceilometer in Beijing during APEC, 2014

G. Tang[1], X. Zhu[1], B. Hu[1], J. Xin[1], L. Wang[1], C. Münkel[2], G. Mao[3], and Y. Wang[1]

[1]State Key Laboratory of Atmospheric Boundary Layer Physics and Atmospheric Chemistry (LAPC), Institute of Atmospheric Physics, Chinese Academy of Sciences, Beijing 100029, China
[2]Vaisala GmbH, Hamburg 22607, Germany
[3]Institute of Meteorology and Climate Research (IMK-IFU), Karlsruhe Institute of Technology (KIT), Kreuzeckbahnstr. 19, 82467 Garmisch-Partenkirchen, Germany

Received: 30 March 2015 – Accepted: 16 April 2015 – Published: 5 May 2015

Correspondence to: Y. Wang (wys@mail.iap.ac.cn)

Published by Copernicus Publications on behalf of the European Geosciences Union.

Abstract

During the 2014 Asia-Pacific Economic Cooperation (APEC) summit, a reduction of air pollution sources was coordinated to ensure good air quality in Beijing and the surrounding provinces and cities. By investigating variations in air pollution during this period, the effects of local emissions and regional transport can be better understood and the information can be used to evaluate the effectiveness of emission reduction strategies and provide a theoretical basis to guide future emission reduction strategies. From 15 October to 30 November 2014, the height of the atmospheric mixing layer and the aerosol attenuated backscattering coefficient profile were observed online using a lidar ceilometer. By investigating the correlation between fine particulate matter ($PM_{2.5}$) data near the surface and attenuated backscattering coefficients measured by the lidar ceilometer as well as the correlation between aerosol optical depth (AOD) and attenuated backscattering coefficients of the 0 to 4500 m column, we found that the attenuated backscattering coefficient measured by the lidar ceilometer is highly correlated with the $PM_{2.5}$ concentration and AOD (correlation coefficients of 0.89 and 0.86, respectively). This result demonstrates the reliability of the vertical profile of aerosols measured by the lidar ceilometer. By analyzing the atmospheric backscattering profile, we found that during the initial stage of pollution accumulation, which is affected by transport of southerly jet flows at low altitude, the attenuated backscattering coefficient of atmospheric aerosols from 0 to 1500 m was greatly enhanced by approximately 1.4 $Mm^{-1}\,sr^{-1}$ (140 %). At the peak pollution stage, the height of the mixing layer gradually decreased, the ratio of CO/SO_2 gradually increased and emissions were dominated by local emissions. The attenuated backscattering coefficient of aerosols from 0 to 300 m suddenly increased, and the aerosols near surface had the highest value (approximately 14 $Mm^{-1}\,sr^{-1}$); however, the attenuated backscattering coefficient of aerosols from 300 to 900 m gradually decreased, and the average value from 0 to 1500 m decreased by 0.5 $Mm^{-1}\,sr^{-1}$ (20 %). By comparing the $PM_{2.5}$ concentrations before, during and after APEC (BAPEC, DAPEC and AAPEC, respectively), we found

ACPD
15, 13173–13209, 2015

that the concentration of fine particles decreased by 60 % and visibility improved by 60 % during APEC. In addition, compared with the BAPEC and AAPEC periods, the contribution of regional transport in the DAPEC period decreased by approximately 36 and 25 %, respectively, and the local contribution decreased by approximately 48 and 54 %, respectively. Thus, the most effective method of controlling air pollution in the Beijing area is to reduce regional emissions during the initial stage of air pollution and reduce local emissions during the peak pollution stage.

1 Introduction

Aerosols are a relatively stable suspension system formed by micro-liquid and solid particles that are uniformly distributed in the air (Seinfeld, and Pandis, 1998). Atmospheric aerosols can directly change the balance and distribution of global radiation by scattering or absorbing sunlight, and they can also affect the formation of clouds and fogs (as condensation nucleus) and indirectly affect the global climate (Shine and Forster, 1999; Myhre et al., 2001; IPCC, 2007). Furthermore, atmospheric aerosols are carriers of photochemical reactions and provide good reaction beds for chemical reactions; therefore, they promote the occurrence of atmospheric photochemical reactions (Seinfeld and Pandis, 1998). Because of the small radii and high specific areas, atmospheric aerosols can be easily accumulated as hazardous material and absorbed by human bodies, where they are deposited in lungs and threaten human health (Englert, 2004; Campbell et al., 2005; Peters, 2005; Auger et al., 2006).

With the rapid economic development in China, the amount of industrial products and number of vehicles continue to increase every year, which increases the energy consumption (National Bureau of Statistics of China, 2014). The North China Plain region has one of the highest global aerosol concentrations (Lu et al., 2010). Beijing is the economic, political and cultural center of China, and it is adjacent to the Yan Mountains to the north and Taihang Mountains to the west and on the north boundary of the North China Plain. Such a special horseshoe-shaped geographical location results in

ACPD
15, 13173–13209, 2015

efficient southerly transport of pollutants to Beijing, which affects the air quality (Ding et al., 2005; Xin et al., 2010). In 2012, China promulgated the "Air Pollution Prevention and Control Action Plan" to prevent and control air pollution, and the details were disseminated in September 2012. The key controlled region for air pollution is the North China Plain, which contains Beijing, Tianjin and Hebei, and the coordinated prevention and control of pollution in this region are proposed (State council, 2013).

Although coordinated regional prevention and control has been proposed for many years, it is difficult to obtain evidence and quantify the intensity of regional transport solely based on ground observations. Thus, reductions in regional emissions have not been implemented. To quantify the intensity and height of regional transport, the vertical gradient of atmospheric pollutants must be measured and the air quality model must be evaluated. However, in previous studies of regional transport based on air quality models, the vertical gradient of air pollutants was not measured to test the model; therefore, the results are not reliable (Wu et al., 2011). Thus, it is of great importance to measure the vertical gradient of air pollutants to quantify regional transport.

Studies of the vertical distribution characteristics of atmospheric aerosols include layered observations from meteorological observation towers, mooring boats, airplanes, ground remote sensing and satellites, and such data can be utilized for exploration and measurements of different spatial regions from the near-surface to high-level atmosphere. Using these observation methods to study the vertical gradient, the effects of sand dusts (Zhang et al., 2006; McAuliffe and Ruth, 2013), volcanic explosions (Emeis et al., 2014), and anthropogenic sources (Tesche et al., 2007; van der Kamp et al., 2008; Zhang et al., 2009; Hänel et al., 2012; Sun et al., 2013) on the atmospheric environment have been evaluated in various countries. However, such studies in North China remain at the initial stages. Using the airplane observation method, Zhang et al. (2006) classified the origin of atmospheric aerosols in Beijing and showed that they are primarily affected by sand dusts, southerly transport and local emissions. Their airplane data were used to determine the concentration of aerosol particles and vertical distribution characteristics of particle radii in the Beijing area during the peri-

ACPD
15, 13173–13209, 2015

ods when atmospheric aerosols are mainly affected by anthropogenic sources. Zhang et al. (2009) also analyzed the causes of vertical aerosol distribution under different meteorological conditions by considering meteorological factors. Guinot et al. (2006) and Sun et al. (2013) used the layered meteorological observation method to show variations in the vertical gradient of air pollutants during periods of heavy pollution. Although the abovementioned studies analyzed the vertical variation of aerosols in the Beijing area, the results are not ideal because they have a low resolution, small sample size and low observational height; are unrepresentative; and lack evidence for regional transport. In recent years, satellite observations have become increasingly important in investigations of atmospheric aerosol profiles. In addition, the satellite observations provide reliable results compared with the ground remote sensing (Wu et al., 2014). However, because of the short passing time and low data resolution of the satellite observation method, surface remote sensing is the best method for determining the vertical structure of atmospheric aerosols.

The Asia-Pacific Economic Cooperation (APEC) summit was held from 3 to 11 November 2014 in Beijing, and it was important to ensure good air quality to provide for a successful summit. Thus, the governments of Hebei Province, Tianjin City, Shanxi Province, Inner Mongolia Province, and Shandong Province cooperated with the government of Beijing to increase the intensity of emissions reductions for the entire region of North China during the APEC summit, and a series of emission reduction methods were conducted. The implementation of these emission reduction methods resulted in significant variations in regional transport and local pollutant contributions, and these data were utilized in the present study, which measured the vertical aerosol profiles and heights of the mixing layers using a lidar ceilometer before and after APEC (15 October to 30 November 2014). The values for fine particulate matter ($PM_{2.5}$) and aerosol optical depth (AOD) were combined, and the present study tested and verified the attenuated backscattering coefficient measured by the lidar ceilometer from 15 October to 30 November 2014 and analyzed the vertical gradients of aerosol concentrations in multiple pollution processes during different pollution periods to determine the origin of

ACPD
15, 13173–13209, 2015

atmospheric aerosols. Changes in the vertical aerosol profiles before, during and after APEC (BAPEC, DAPEC and AAPEC, respectively) reflect the causes of variation during different pollution periods and relative contribution of regional transpo[illegible]nd local emissions in the DAPEC period. Finally, three typical pollution processes were analyzed in the BAPEC, DAPEC and AAPEC periods to show the origin of atmospheric fine particles in different pollution periods in Beijing and the effects of the emission reduction methods in the DAPEC period. The results strengthen our knowledge of pollution formation and development in the Beijing area and provide a scientific basis for the control of air pollution in Beijing.

2 Methods

2.1 Measurements of aerosol attenuated backscattering coefficients

An observational station was built in the Tieta courtyard of the Institute of Atmospheric Physics of the Chinese Academy of Science (West of Jiandemen, Haidian District, Beijing). The station is between North Third Ring Road and North Fourth Ring Road, and route G6 is on the east side. The geographic location of the station is 39.97° N, 116.37° E, and the altitude is 60 m.

The equipment used in this study included an enhanced single-lens lidar ceilometer (CL51, Vaisala). This equipment adopts the strobe laser lidar (laser detection and distance measurement) technique (910 nm) to measure the attenuated backscattering coefficient profiles of atmospheric particles. The detection distance of the CL51 ceilometer is 15.4 km, and it has a temporal resolution of 6–120 s and vertical resolution of 10 m. Because the height of the atmospheric mixing layer barely exceeds 4 km and the concentration of aerosols in the high-level atmosphere above the mixing layer is low in the Beijing area, high detection distance is not necessary to study the air pollution in this area. To strengthen the echo signals and reduce detection noise, the detection height of the ceilometer was reduced by half to 7.7 km. Additional data were

ACPD
15, 13173–13209, 2015

obtained to smooth the noise of detection signals by setting the temporal resolution of detection to 16 s.

2.2 Validation method of attenuated backscattering coefficients

Uncertainties might occur in the attenuated backscattering coefficients measured by the lidar ceilometer, especially above the boundary layer where the aerosol concentration is low (Jin et al., 2015). To verify the atmospheric attenuated backscattering coefficients measured by the lidar ceilometer, two methods based on the near-surface $PM_{2.5}$ concentration and AOD column data were adopted in this study. The reliability of measured results based on calibration of near-surface attenuated backscattering coefficients was verified by comparing the near-surface $PM_{2.5}$ concentrations and near-surface atmospheric attenuated backscattering coefficients. Observational $PM_{2.5}$ data were downloaded from the Chinese Environmental Protection Administration website (http://www.zhb.gov.cn/), and observational data at the Olympic Center, which is the closest landmark to the observational station, were chosen for comparison. The AOD data were measured using the MICROTOPS II heliograph, and the weather conditions were sunny and partly cloudy. Each measurement was repeated three to five times, and the average value was used as the mean value at each time step. Because the waveband of the heliograph is different from the observational range of the lidar ceilometer, the AOD at 910 nm, which is consistent with the wavelength of the lidar ceilometer, was derived from the measured AOD at 1020 nm using the heliograph and wavelength indices of four wave bands. The derivation method is based on Eq. (1), where α is the wavelength index between 340 and 675 nm, and τ is AOD:

$$\ln\alpha = \frac{\ln\tau(1020\,\mathrm{nm}) - \ln\tau(910\,\mathrm{nm})}{\ln 1020 - \ln 910} \quad (1)$$

ACPD
15, 13173–13209, 2015

2.3 Method to calculate mixing layer height

Because the particle lifetimes are long and range from several days to tens of days, the distribution of particle concentrations in the atmospheric mixing layer is more uniform than that of gas-phase pollutants (Seinfeld, and Pandis, 1998). In addition, huge differences are observed in the concentrations of particles in the mixing layer and free atmosphere. The profile of attenuated backscattering coefficients in the atmosphere can be analyzed to determine the location of sudden changes caused by variations in the attenuated backscattering coefficients, which is at the top of the atmospheric mixing layer. The lidar ceilometer is low-cost and convenient and has been widely applied in observations of the mixing layer height (Michael et al., 2006; Münkel et al., 2007; McKendry et al., 2009; Emeis et al., 2012; Yang et al., 2013; Pandolfi et al., 2013; Schween et al., 2014; Scarino et al., 2014). In this study, the gradient method is used to identify the mixing layer height, and maximum negative gradient value ($-\mathrm{d}\beta/\mathrm{d}x$) of the attenuated backscattering coefficient profile of aerosols is at the top of the mixing layer (Michael et al., 2006; Emeis et al., 2012). Because the data are easily affected by noise and interference from the aerosol layering structure, time or space must be smoothly averaged before the improved gradient method can be used to calculate the mixing layer height from the averaged profile data (Münkel et al., 2007).

2.4 Other data

Because Beijing has a low concentration of industry and a large quantity of vehicle traffic, the emissions of SO_2 are low while the emissions of CO are high. Thus, the ratio of CO to SO_2 may provide a partial indication of the origin of atmospheric pollutants. The CO and SO_2 data at the Olympic Center published by the Chinese Environment Protection Administration were also used to help analyze the origin of atmospheric pollutants. The observational data were downloaded from the live-updated website published by the Chinese Environment Protection Administration (http://www.zhb.gov.cn/).

ACPD
15, 13173–13209, 2015

To understand the transport characteristics of different atmospheric pollution stages, vertical profile data of wind speeds and directions are required. Meteorological data were obtained from the website of the University of Wyoming, and meteorological sounding data were measured twice a day at 08:00 and 20:00 LT (http://weather.uwyo.edu).

3 Result and discussion

3.1 Characteristics of variations in $PM_{2.5}$ concentration

During the summit, a number of controls were adopted to guarantee good air quality in Beijing. To understand the pollution variation tendency during this period of time, the $PM_{2.5}$ concentration was plotted against time using the hourly $PM_{2.5}$ concentration data from 15 October to November (Fig. 1). The observation period lasted for 47 days, and 9 pollution processes were observed, each of which lasted for 5.2 days on average. During each pollution process, the $PM_{2.5}$ concentration was characterized as "slowly accumulating and rapidly disappearing". At the pollution accumulation stage during each pollution process, the pollutant concentration increased. After reaching the maximum value, the pollutant concentration rapidly decreased, which usually lasted for four to six days from the beginning of the pollution process to the end. This result is consistent with that of previous studies (Jia et al., 2008).

A statistical analysis of the ground concentrations of $PM_{2.5}$ and heights of the mixing layers at the same time showed that with mixing layer heights rising from 0 to 1000 m, the average $PM_{2.5}$ concentration decreased from 158.9 to 67.9 $\mu g\,m^{-3}$. When mixing layer heights rose above 1200 m, the $PM_{2.5}$ concentration suddenly decreased (lower than 35 $\mu g\,m^{-3}$) and did not vary with increasing height of the mixing layer (Fig. 2). Thus, when the mixing layer was lower than 1000 m, the $PM_{2.5}$ concentration was negatively correlated with the mixing-layer height, and when the mixing layer was above 1000 m, the air was of good quality and the negative correlation between the $PM_{2.5}$ con-

ACPD
15, 13173–13209, 2015

centration and mixing-layer height disappeared. Therefore, increased pollution during each pollution process gradually leads to the accumulation of $PM_{2.5}$ above 60 $\mu g\,m^{-3}$, and the corresponding mixing layer heights are all below 1000 m. This result indicates that the vertical diffusion capability of the atmosphere is weak, and atmospheric pollution in Beijing is possibly enhanced by local emissions. Because the level of industry and coal pollution is low and the number of vehicles is high in Beijing, the ratio of CO/SO_2 can reflect the contribution of local emissions to air pollution, with higher ratios indicating higher local contributions. The ratios of CO/SO_2 were calculated and they show that with decreasing mixing layer height, the ratio of CO/SO_2 gradually increases. This result also suggests that with increasing pollution, the amount of pollutants transported from other regions gradually decreases while the local contribution gradually increases.

3.2 Characteristics of the vertical structure variation of atmospheric aerosols

3.2.1 Validation of the attenuated backscattering coefficient profile

Because the vertical distribution of atmospheric pollutants in the convective layer can better represent the evaluation characteristics of pollution, the $PM_{2.5}$ and AOD data observed during this time period were used to compare the near-surface atmospheric attenuated backscattering coefficient and 0 to 4500 m column attenuated backscattering coefficient, and the results could be used to verify the attenuated backscattering coefficient profile of atmospheric aerosols measured by the lidar ceilometer and help us to better understand the vertical structure of atmospheric aerosols.

Overlap of the laser beam of the ceilometer and its receiver field-of-view is smaller than 1 in the near range. Therefore in this paper the attenuated backscattering coefficient values at 100 m height have been chosen for the comparison with near-surface $PM_{2.5}$ concentration. The correlation showed that in addition to differences during several peak periods, the variations were generally consistent (Fig. 3a), which indicates that the attenuated backscattering coefficients above 100 m and corresponding $PM_{2.5}$

ACPD
15, 13173–13209, 2015

concentrations are significantly positively correlated (R = 0.89) (Fig. 3b). For the column concentration, 4500 m can generally cover the entire mixing layer; therefore, the interference of cloud layers from 0 to 4500 m was manually removed and attenuated backscattering coefficients of atmosphere were integrated in this region, and the values were compared with the AOD concentration. The results showed that the AOD concentration varied directly with the integrated attenuated backscattering coefficient of the atmospheric column (Fig. 4a), and the positive correlation coefficient was as high as 0.86 (Fig. 4b). Thus, the significant correlations between the attenuated backscattering coefficient of aerosols and concentrations of fine particles and the AOD show that the vertical attenuated backscattering coefficient profile measured by the lidar ceilometer could accurately represent the vertical structure of atmospheric aerosols.

3.2.2 Vertical structure of atmospheric aerosols

Figure 5 shows variations in the average vertical gradient of atmospheric aerosols during the period of observation. The figure shows clear differences among the attenuated backscattering coefficients of the atmospheric aerosols, with the highest values at the near-surface atmosphere and average values reaching 4.5 $Mm^{-1}\,sr^{-1}$. The vertical decline of the attenuated backscattering coefficients for layers from 0 to 200 m was small, and the attenuated backscattering coefficients showed limited variation; however, the vertical decline above 200 m increases and the attenuated backscattering coefficients significantly decrease. After reaching the maximum value at the height of 400 to 800 m, the vertical decline began to gradually decrease. Above 1000 m, the attenuated backscattering coefficient was lower than 0.65 $Mm^{-1}\,sr^{-1}$, and at approximately 2000 m, the coefficient was lower than 0.1 $Mm^{-1}\,sr^{-1}$. A vertical gradient with high values below and low values above is consistent with the characteristics of vertical gradient variations in other cities and regions (Tesche et al., 2007; Zhang et al., 2009; Liu et al., 2012; Cao et al., 2013; McAuliffe and Ruth, 2013), although it is different from those of regions that are severely affected by regional transport (Yang et al., 2007). Thus, the gradual declining trend in the attenuated backscattering coefficient

ACPD
15, 13173–13209, 2015

from near-surface to high-level atmospheric layers indicates that the main sources of atmospheric aerosols are from the near-surface layers.

3.2.3 Variation in the vertical gradient of atmospheric aerosols during different pollution stages

Although the main sources of atmospheric aerosols are from the near-surface layers, fine particles originate from different locations in the pollution stages of each pollution process. Visibility was used as an index to indicate the degree of air pollution and applied in the analysis of the vertical gradient profile of the attenuated backscattering coefficients under different visibility conditions (Fig. 6). When the visibility was above 40 km, small differences occurred in the vertical gradients of the aerosol attenuated backscattering coefficients from the ground to 1.5 km, and the corresponding attenuated backscattering coefficients were all below 2 $Mm^{-1}\,sr^{-1}$. With decreasing visibility, the attenuated backscattering coefficients increased to varying degrees from the ground to 1.0 km. The near-ground layer presented a 2.1-fold increase from 2.4 to 7.4 $Mm^{-1}\,sr^{-1}$ when the visibility decreased from 20 to 4 km, and the mean attenuated backscattering coefficient from 0 to 1500 m presented a 1.4-fold increase from 1 to 2.4 $Mm^{-1}\,sr^{-1}$. In addition, the highly polluted region shifted from 0 to 300 to 0 to 900 m, indicating that transport in high-level atmospheric layers played an important role from the clean stage to the initial accumulation stage with medium haze. When the visibility decreased from 4 to 1 km, the backscatter coefficient of aerosols near the surface varied from 7.4 to 14 $Mm^{-1}\,sr^{-1}$, which was almost double. However, the mean attenuated backscattering coefficient from 0 to 1500 m significantly decreased from 2.4 to 1.9 $Mm^{-1}\,sr^{-1}$ (approximately 20 %). The significant decrease in the mean column concentration differed from the rapid increase of the near-surface concentration. The attenuated backscattering coefficient from 300 to 900 m significantly decreased and the variation at approximately 450 m reached the maximum value (decreased by approximately 4 $Mm^{-1}\,sr^{-1}$), resulting in a sudden shift of the near-surface high concentration region from 0 to 900 m to 0 to 300 m. Such a phenomenon is primarily caused by the

ACPD
15, 13173–13209, 2015

weakened transport capability of atmosphere during the heavy haze, which results in decreased concentrations in the high level atmosphere, and the increased contributions of local pollutants leads to a sudden increase of pollutant concentrations. Thus, during the initial increasing stage of pollution, regional transport plays an important role, and within 0 to 600 m, it is characterized by strong regional transport. During the peak pollution stage, local emissions are the most important factor and determine the accumulation rate of pollutants and pollution intensity.

3.3 Evaluation of emission reduction controls during APEC

To evaluate the effectiveness of the emission reduction strategies during APEC, the observation periods were divided into three parts: BAPEC (15 October to 2 November), DAPEC (3 to 12 November) and AAPEC (13 to 30 November). A statistical analysis of the $PM_{2.5}$ concentration during these three time periods (Table 1) showed that the $PM_{2.5}$ concentrations in the BAPEC, DAPEC and AAPEC periods were 126.8, 51.5 and 125.2 $\mu g\,m^{-3}$, respectively. Compared with the concentrations of BAPEC and AAPEC, the $PM_{2.5}$ concentration in the DAPEC period was decreased by approximately 60 %. Correspondingly, the visibility was increased from 17.5 km in the BAPEC period and 19.1 km in the AAPEC period to 29.8 km in the DAPEC period, which is an increase of approximately 60 %. To evaluate the diffusion capability of the atmosphere during these three periods of time, the corresponding wind speeds and mixing-layer heights were calculated. The wind speeds in the BAPEC, DAPEC, and AAPEC periods were 2.4, 3.1 and 2.6 $m\,s^{-1}$, respectively, and the mixing-layer heights were 502.3, 452.8 and 423.9 m, respectively. Because wind speeds and mixing layer heights can represent atmospheric diffusion capacity along the horizontal and vertical direction, respectively, the ventilation coefficient (wind speed multiplied by the mixing layer height) was used as an index to evaluate the total diffusion capacity of the atmosphere. The ventilation coefficients in the BAPEC, DAPEC, and AAPEC periods were 1208.3, 1400.0 and 1085.9 $m^2\,s^{-1}$, respectively. Thus, the diffusion capability of the atmosphere in the DAPEC period was the best, but the variation magnitude was far below the decreased

ACPD
15, 13173–13209, 2015

magnitude of the fine particles, which indicates that coordinated regional emission reductions might have caused the significant decrease in fine particle concentration in the atmosphere.

The results in Sects. 3.1 and 3.2 show that fine particles originate from different sources during different pollution stages. In order to identify the vertical gradient variations during different pollution stages in the BAPEC, DAPEC and AAPEC periods, the $PM_{2.5}$ concentration was divided as follows: 50, 50 to 100 and > 100 $\mu g\,m^{-3}$, which represented the clean period, accumulation period and peak period, respectively. The vertical gradient variations of the atmospheric attenuated backscattering coefficients under the three different pollution concentrations were statistically analyzed to obtain the attenuated backscattering coefficient profile plots for the three periods of time (Fig. 7).

During the clean period, the attenuated backscattering coefficients for the BAPEC, DAPEC, and AAPEC periods from 0 to 2000 m were similar, and the coefficients for the near surface were all below 1.5 $Mm^{-1}\,sr^{-1}$. The near-surface attenuated backscattering coefficients in the AAPEC period was higher than those during other periods by 0.3 $Mm^{-1}\,sr^{-1}$ because of wide-spread heating after 15 November. The variation magnitude was approximately 20 %.

Because of the important effect of regional transport from 0 to 1000 m, the attenuated backscattering coefficients were all higher during the initial pollution accumulation stage compared with that of the clean stage for all three periods of time, with 1.2- to 3-fold changes at different heights. Interestingly, compared with other periods, greater decreases in the coefficients occurred in the DAPEC period with increasing height, and at 1000 m, the value was approximately 35 and 25 % higher compared with that of BAPEC and AAPEC, respectively. The smallest decrease of attenuated backscattering coefficients occurred near the surface at only 10 %. The decreased pollutant concentration in the upper air relative to the near surface showed that during the initial pollutant accumulation stage, regional transport was an important contributor to air pollution in Beijing. Considering the dominant effect of regional transport during this stage and jet flow transport in the lower atmosphere within 300 to 900 m, the mean

ACPD
15, 13173–13209, 2015

attenuated backscattering coefficient of atmospheric aerosols in the DAPEC, BAPEC, and AAPEC periods was calculated to eliminate the effect of local emission. The results showed that the attenuated backscattering coefficient for the DAPEC period decreased by 36 and 25 % relative to the BAPEC and AAPEC, respectively; thus, the contribution of regional transport to atmospheric aerosols in Beijing decreased by approximately 36 and 25 %, respectively.

Compared with the initial accumulation stage, the near-surface attenuated backscattering coefficients for the DAPEC, AAPEC and BAPEC periods were all greatly enhanced during the heavy pollution stage and began to decrease at 600 to 1000 m. The near-surface attenuated backscattering coefficients in the BAPEC and AAPEC periods exceeded 8 $Mm^{-1}\,sr^{-1}$, which was approximately twice of the variation that occurred in the initial accumulation stage. The near-surface attenuated backscattering coefficient at the DAPEC peak stage was only 4 $Mm^{-1}\,sr^{-1}$, and the increase compared to the initial accumulation stage was 25 %. Compared with that of the BAPEC and AAPEC, the attenuated backscattering coefficients in the DAPEC period were decreased by 0 to 48 % and 0 to 54 %, respectively, and the near-surface attenuated backscattering coefficients showed the greatest decrease at 48 and 54 %, respectively. With the increase of height, the decreasing magnitude of the attenuated backscattering coefficients gradually decreased. The higher decreasing magnitude of the near-surface level relative to higher atmospheric levels indicates that during the peak pollution period, local emission contributed significantly to air pollution. Considering the dominant role of local emissions during this period of time and using the near-surface attenuated backscattering coefficient as a baseline, the significant decreases in the DAPEC period relative to the BAPEC and AAPEC periods indicate that the contribution of local emissions decreased by 48 and 54 %, respectively.

Although a number of air pollution controls were implemented during the DAPEC period, the increased heat supply is the only difference between BAPEC and AAPEC. To evaluate the effect of heat supply on air pollution during the heavy haze periods in Beijing, the near-surface aerosol attenuated backscattering coefficients in the BAPEC and

ACPD
15, 13173–13209, 2015

AAPEC periods were compared, and the result showed that they were 1.1-fold higher in the AAPEC period compared with that of the BAPEC period, which indicates that the contribution from the heat supply to atmospheric aerosols in Beijing is approximately 10 %.

Based on the above discussion, three conclusions can be drawn: (1) the regional transport in the DAPEC period decreased by 25 and 36 % compared with BAPEC and AAPEC, respectively, (2) the contribution of local emissions in the DAPEC period decreased by 48 and 54 % compared with that of BAPEC and AAPEC; and (3) the contribution of the local heat supply to atmospheric aerosols in Beijing was approximately 10 %. Although the quantitative contributions of local and regional areas are given, it is still a rough estimate for the different episode. Detailed contributions of local and regional sources over Northern China still need further investigation and additional observational and modeling studies (although beyond the scope of the present analysis) are suggested for further work.

3.4 Pollution variation characteristics during heavy pollution processes

To predict the occurrence and development of air pollution at different stages in Beijing more precisely, the atmospheric attenuated backscattering coefficients, mixing layer height, ratio of CO to SO_2 during the BAPEC, DAPEC, and AAPEC periods and backscattering profile of atmospheric aerosols and wind vectors during typical periods (Figs. 8–13) were evaluated in a time-series plot to investigate the characteristics of variation and causes of attenuated backscattering coefficients during different pollution stages at different heights. The heavy pollution processes in the BAPEC and AAPEC periods (Figs. 8, 9, 12 and 13) showed that during the initial accumulation stage (21–23 October and 17–18 November), southerly low-level jet flow resulted in increased mixing-layer height and a gradual increasing the atmospheric attenuated backscattering coefficient from the near-surface (100 m) to high-level atmosphere (300 to 900 m). From 300 to 800 m, the effect of the southerly low-level jet flow was significant, and the pollutant concentration rapidly increased. However, during the pollution

ACPD
15, 13173–13209, 2015

maintenance stage (23–25 October and 19–20 November), the southerly low-level jet flow disappeared. Thus, the mixing-layer height decreased because of the westerly and northerly jet flows and the attenuated backscattering coefficient of the high-layer atmosphere began to decrease. The reduction in mixing-layer height and relatively low wind speed promoted an increase in near-surface pollutants, which quantitatively accumulated during the peak pollution period. When the pollution was dissipated, the attenuated backscattering coefficient and CO/SO_2 ratio in the lower and upper air both rapidly decreased with the rapidly increased mixing layer height, and the $PM_{2.5}$ in the atmosphere was significantly decreased. Subsequently, the entire pollution process was completed. Although the mixing layer height gradually decreased, the "slow accumulation and rapid disappearance" characteristics of the fine-particle concentration, which were obvious in the BAPEC and AAPEC periods, were not clear in the pollution process in the DAPEC period (6–11 October). In addition, variations in the $PM_{2.5}$ concentration and atmospheric attenuated backscattering coefficient appeared as zigzag shapes, and accumulation and disappearance alternated (Fig. 10). At the initial accumulation stage in the DAPEC period, the variations of air pollutants were similar to those of the BAPEC and AAPEC. Because of the effect of the southerly low-level jet flow, the simultaneous increase from low- to high-layer atmosphere that occurred in the BAPEC and AAPEC also occurred in the DAPEC period (Figs. 10 and 11). In addition, the ratio of CO to SO_2 was low, indicating that regional transport was dominant during this period of time. At the pollution maintenance stage, the attenuated backscattering coefficient of the upper air in the DAPEC period significantly decreases because of the disappearance of westerly jet flows, which is consistent with what occurred in the BAPEC and AAPEC periods. However, the near-surface attenuated backscattering coefficient did not show a sharp increase (up and down), and the CO/SO_2 ratio did not increase as expected. Instead, the near-surface attenuated backscattering coefficient decreased. Thus, at the peak pollution stage in the DAPEC period, the decreased local contribution magnitude of pollutants was insufficient to maintain the increases of

ACPD
15, 13173–13209, 2015

pollutant concentrations at the near surface, which resulted in a zigzag distribution of atmospheric attenuated backscattering coefficients at the pollutant accumulation stage.

Based on the above discussion, southerly low-level jet flow occurred in the initial accumulation stage (21–22 October, 7–8 November, 17–18 November) in the high-level atmosphere (300 to 900 m), and they transported large quantities of pollutants from the south to Beijing. In turn, the attenuated backscattering coefficients in the low- and high-layer atmosphere increased, and the abundance of pollutants in the mixing layer increased. Pollutants transported during the daytime are mixed with pollutants released locally because of the turbulence, and pollutants transported at night remain above the mixing layer overnight and then move to the near surface through high atmosphere convection after the development of the mixing layer. Because of the transportation effect, the variation rate of the entire profile was relatively small and resulted in increased column concentrations of pollutants throughout the layer, which lead to the air pollution. At the peak pollution stage (24–26 October, 8–11 November and 19–21 November), low-level jet flow were not significant, and they were replaced by near-surface static winds and westerly and northerly winds in the high layers. Because of this effect, the near-surface attenuated backscattering coefficient continued to increase, whereas that of the high-layer atmosphere continued to decrease, resulting in increased variation rates of the entire profile with height. The contribution of local emissions to pollution at the peak pollution stage increased, and its contribution to the high-layer atmosphere was reduced.

4 Conclusions

The APEC summit was held in Beijing from 3 to 11 November 2014. During this period, six provinces near Beijing (Beijing, Tianjin, Hebei, Shanxi, Inner Mongolia, and Shandong) worked together to control the air pollution by emission reduction, and this period provides the best experimental platform for studying regional pollution and transport. The following conclusions have been drawn based on the backscattering profile of the

ACPD
15, 13173–13209, 2015

atmospheric aerosols and mixing layer height in the Beijing area as measured by the lidar ceilometer for the period 15 October to 30 November 2014.

1. A comparison of the $PM_{2.5}$ concentrations and AOD values showed that the near-surface and 0 to 4500 m attenuated backscattering coefficient measured by the lidar ceilometer were well correlated with the near-surface $PM_{2.5}$ and AOD values, respectively, indicating that the lidar ceilometer can be used to study air pollution and indicate regional transport characteristics of atmospheric aerosols in high layers.

2. Air pollutants at different stages in Beijing are from different sources. The initial stage is primarily affected by southerly low-level jet flow, and pollutant transport in the 300 to 900 m atmosphere is significant, which results in the accumulation of pollutants and air pollution in Beijing. However, at the peak pollution stage, the contribution of high-layer transport is decreased and local contributions play an important role.

3. $PM_{2.5}$ concentrations in the DAPEC period in Beijing were affected by coordinated regional emission reductions and decreased by approximately 30 %, and the visibility was enhanced by 60 %. At the initial increasing stage, the concentration was mainly affected by regional transport, and the contribution of regional transport to aerosols in the Beijing area was decreased by 36 and 25 %, respectively. At the peak pollution stage, the concentration was dominated by local contributions, and the local contribution in Beijing was significantly decreased by 48 and 54 % relative to the BAPEC and AAPEC periods. A comparison of the near-surface attenuated backscattering coefficients in the BAPEC and AAPEC periods showed that the contribution of the heat supply to air pollution during the heavy haze period was approximately 10 %.

Therefore, local emissions are the key factors for determining the formation and development of air pollution in the Beijing area, and a reduction in local emissions can

ACPD
15, 13173–13209, 2015

greatly decrease local pollution. However, regional transport can promote air pollution; therefore, such processes cannot be ignored, particularly at the initial pollution stage, which results in enhanced intensity and increased accumulation of local pollution. Thus, at the initial pollution stage, the emissions in areas surrounding Beijing should be reduced to effectively control regional transport and reduce the load of regional pollution. At the peak pollution stage, local emissions should be reduced to control pollution. Our results can provide a scientific basis for emission control and management and air pollution forecasting and prevention and have the potential for use in the design and implementation of coordinated regional reduction strategies.

Acknowledgements. This work was supported by National Natural Science Foundation of China (nos. 41230642 and 41222033) and the CAS Strategic Priority Research Program Grant (no. XDB05020000 and XDA05100100).

References

Auger, F., Gendron M.-C., Chamot, C., Marano, F., and Dazy A.-C.: Responses of well-differentiated nasal epithelial cells exposed to particles: role of the epithelium in airway inflammation, Toxicol. Appl. Pharm., 215, 285–294, 2006.

Campbell, A., Oldham, M., Becaria, A., Bondy, S. C., Meacher, D., Sioutas, C., Misra, C. Mendez L. B., and Kleinman, M.: Particulate matter in polluted air may increase biomarkers of inflammation in mouse brain, NeuroToxicology, 26, 133–140, 2005.

Cao, X., Wang, Z., Tian, P., Wang, J., Zhang, L., and Quan, X.: Statistics of aerosol extinction coefficient profiles and optical depth using lidar measurement over Lanzhou, China since 2005–2008, J. Quant. Spectrosc. Radiat. Transfer., 122, 150–154, 2013.

Ding, G. A., Chen, Z. Y., Gao, Z. Q., Yao, W. Q., Li, Y., Cheng, X. H., Meng, Z. Y., Yu, H. Q., Wong, K. H., Wang, S. F., and Miao, Q. J.: Vertical structures of PM_{10} and $PM_{2.5}$ and their dynamical character in low atmosphere in Beijing urban areas, Sci. China Ser. D-Earth Sci., 35, 31–44, 2005.

Emeis, S., Forkel, R., Junkermann, W., Schäfer, K., Flentje, H., Gilge, S., Fricke, W., Wiegner, M., Freudenthaler, V., Groß, S., Ries, L., Meinhardt, F., Birmili, W., Münkel, C., Obleitner, F., and Suppan, P.: Measurement and simulation of the 16/17 April 2010 Eyjafjallajökull

ACPD
15, 13173–13209, 2015

volcanic ash layer dispersion in the northern Alpine region, Atmos. Chem. Phys., 11, 2689–2701, doi:10.5194/acp-11-2689-2011, 2011.
Emeis, S., Schäfer, K., Münkel, C., Friedl, R., and Suppan, P.: Evaluation of the interpretation of ceilometer data with RASS and radiosonde data, Bound.-Lay. Meteorol., 143, 25–35, 2012.
Englert, N.: Fine particles and human health-a review of epidemiological studies, Toxicol. Lett., 149, 235–242, 2004.
Guinot, B., Roger, J.-C., Cachier, H., Pucai, W., Jianhui, B., and Tong, Y.: Impact of vertical atmospheric structure on Beijing aerosol distribution, Atmos. Environ., 40, 5167–5180, 2006.
Hänel, A., Baars, H., Althausen, D., Ansmann, A., Engelmann, R., and Sun, J. Y.: One-year aerosol profiling with EUCAARI Raman lidar at Shangdianzi GAW station: Beijing plume and seasonal variations, J. Geophys. Res., 117, D13201, doi:10.1029/2012JD017577, 2012.
IPCC: Cimate Change 2007: Synthesis Report, Contribution of Working Groups I, II and III to the Fourth Assessment Report of the Intergovernmental Panel on Climate Change Geneva, IPCC, Switzerland, 2007.
Jia, Y., Rahn, K. A., He, K., Wen, T., and Wang, Y.: A novel technique for quantifying the regional component of urban aerosol solely from its sawtooth cycles, J. Geophys. Res., 113, D21309, doi:10.1029/2008JD010389, 2008.
Liu, J., Zheng, Y., Li, Z., Flynn, C., and Cribb, M.: Seasonal variations of aerosol optical properties, vertical distribution and associated radiative effects in the Yangtze Delta region of China, J. Geophys. Res., 117, D00K38, doi:10.1029/2011JD016490, 2012.
Lu, Z., Streets, D. G., Zhang, Q., Wang, S., Carmichael, G. R., Cheng, Y. F., Wei, C., Chin, M., Diehl, T., and Tan, Q.: Sulfur dioxide emissions in China and sulfur trends in East Asia since 2000, Atmos. Chem. Phys., 10, 6311–6331, doi:10.5194/acp-10-6311-2010, 2010.
McAuliffe, M. A. P. and Ruth, A. A.: Typical tropospheric aerosol backscatter profiles for Southern Ireland: the Cork Raman lidar, Atmos. Res., 120–121, 334–342, 2013.
McKendry, I. G., van der Kamp, D., Strawbridge, K. B., Christen, A., and Crawford, B.: Simultaneous observations of boundary-layer aerosol layers with CL31 ceilometer and 1064/532 nm lidar, Atmos. Environ., 43, 5847–5852, 2009.
Münkel, C., Eresmaa, N., Räsänen, J., and Karppinen, A.: Retrieval of mixing height and dust concentration with lidar ceilometers, Bound.-Lay. Meteorol., 124, 117–128, 2007.
Myhre, G., Myhre, A., and Stordal, F.: Historical evolution of radiative forcing of climate, Atmos. Environ., 35, 2361–2373, 2001.

ACPD
15, 13173–13209, 2015

National Bureau of Statistics of China: China Statistical Yearbook 2014, available at: http://www.stats.gov.cn/tjsj/ndsj/2014/indexch.htm (last access: 16 January 2015), China Statistics Press, Beijing, 2014.

Pandolfi, M., Martucci, G., Querol, X., Alastuey, A., Wilsenack, F., Frey, S., O'Dowd, C. D., and Dall'Osto, M.: Continuous atmospheric boundary layer observations in the coastal urban area of Barcelona during SAPUSS, Atmos. Chem. Phys., 13, 4983–4996, doi:10.5194/acp-13-4983-2013, 2013.

Peters, A.: Particulate matter and heart disease: evidence from epidemiological studies, Toxicol. Appl. Pharm., 207, 477–482, 2005.

Scarino, A. J., Obland, M. D., Fast, J. D., Burton, S. P., Ferrare, R. A., Hostetler, C. A., Berg, L. K., Lefer, B., Haman, C., Hair, J. W., Rogers, R. R., Butler, C., Cook, A. L., and Harper, D. B.: Comparison of mixed layer heights from airborne high spectral resolution lidar, ground-based measurements, and the WRF-Chem model during CalNex and CARES, Atmos. Chem. Phys., 14, 5547–5560, doi:10.5194/acp-14-5547-2014, 2014.

Schween, J. H., Hirsikko, A., Löhnert, U., and Crewell, S.: Mixing-layer height retrieval with ceilometer and Doppler lidar: from case studies to long-term assessment, Atmos. Meas. Tech., 7, 3685–3704, doi:10.5194/amt-7-3685-2014, 2014.

Seinfeld, J. H. and Pandis, S. N.: Atmospheric Chemistry and Physics, From Air Pollution to Climate Changes, Wiley, New York, USA, 1326 pp., 1998.

Shine, K. P. and Forster P. M. F.: The effect of human activity on radiative forcing of climate change: a review of recent developments, Global Planet. Change, 20, 205–225, 1999.

Sicard, M., Perez, C., Rocadenbosch, F., Baldasano, J. M., and Garcia-Vizcaino, D.: Mixed-layer depth determination in the Barcelona coastal area from regular lidar measurements: methods, results and limitations, Bound.-Lay. Meteorol., 119, 135–157, 2006.

State Council: Air Pollution Prevention and Control Action Plan. China Clean Air Updates, no. GUOFA[2013]37, 2013.

Sun, Y., Song, T., Tang, G., and Wang, Y.: The vertical distribution of $PM_{2.5}$ and boundary-layer structure during summer haze in Beijing, Atmos. Environ., 74, 413–421, 2013.

Tesche, M., Ansmann, A., Müller, D., Althausen, D., Engelmann, R., Hu, M., and Zhang, Y.: Particle backscatter, extinction, and lidar ratio profiling with Raman lidar in south and north China, Appl. Optics, 46, 6302–6308, 2007.

ACPD
15, 13173–13209, 2015

van der Kamp, D., McKendry, I. G., Wong, M., and Stull, R.: Lidar ceilometer observations and modeling of a fireworks plume in Vancouver, British Columbia, Atmos. Environ., 42, 7174–7178, 2008.
Wu, Q. Z., Wang, Z. F., Gbaguidi, A., Gao, C., Li, L. N., and Wang, W.: A numerical study of contributions to air pollution in Beijing during CAREBeijing-2006, Atmos. Chem. Phys., 11, 5997–6011, doi:10.5194/acp-11-5997-2011, 2011.
Wu, Y., Cordero, L., Gross, B., Moshary, F., and Ahmed, S.: Assessment of CALIPSO attenuated backscatter and aerosol retrievals with a combined ground-based multi-wavelength lidar and sunphotometer measurement, Atmos. Environ., 84, 44–53, 2014.
Xin, J., Wang, Y., Tang, G., Wang, L., Sun, Y., Wang, Y. H., Hu, B., Song, T., Ji, D. S., Wang, W. F., Li, L., and Liu, G. R.: Variability and reduction of atmospheric pollutants in Beijing and its surrounding area during the Beijing 2008 Olympic Games, Chinese Sci. Bull., 55, 1937–1944, 2010.
Yang, D. W., Li, C., Lau, A. K.-H., and Li, Y.: Long-term measurement of daytime atmospheric mixing layer height over Hong Kong, J. Geophys. Res. Atmos., 118, 2422–2433, 2013.
Yoshitaka, J., Kenji, K., Kei, K., Tomohiro, N., Tetsu, S., Akihiro, Y., Akihiro, U., Dashdondog, B., Nobuo, S., and Tomoaki, N.: Ceilometer calibration for retrieval of aerosol optical properties, J. Quant. Spectrosc. Ra., 153, 49–56, 2015.
Young, M. N., Young, J. K., Byoung, C. C., and Toshiyuki, M.: Aerosol lidar ratio characteristics measured by a multi-wavelength Raman lidar system at Anmyeon Island, Korea, Atmos. Res., 86, 76–87, doi:10.1016/j.atmosres.2007.03.006, 2007.
Zhang, Q., Zhao, C., Tie, X., Wei, Q., Huang, M., Li, G., Ying, Z., and Li, C.: Characterizations of aerosols over the Beijing region: a case study of aircraft measurements, Atmos. Environ., 40, 4513–4527, 2006.
Zhang, Q., Ma, X., Tie, X., Huang, M., and Zhao, C.: Vertical distributions of aerosols under different weather conditions: analysis of in-situ aircraft measurements in Beijing, China, Atmos. Environ., 43, 5526–5535, 2009.

ACPD
15, 13173–13209, 2015

Table 1. Meteorological conditions and atmospheric particle concentrations during different periods of APEC.

	WS ($m\,s^{-1}$)	MLH (m)	Ventilation coefficient ($m^2\,s^{-1}$)	Visibility (km)	$PM_{2.5}$ ($\mu g\,m^{-3}$)
BAPEC	2.4	502.3	1208.3	17.5	126.8
DAPEC	3.1	452.8	1400.0	29.8	51.5
AAPEC	2.6	423.9	1085.9	19.1	125.2

ACPD
15, 13173–13209, 2015

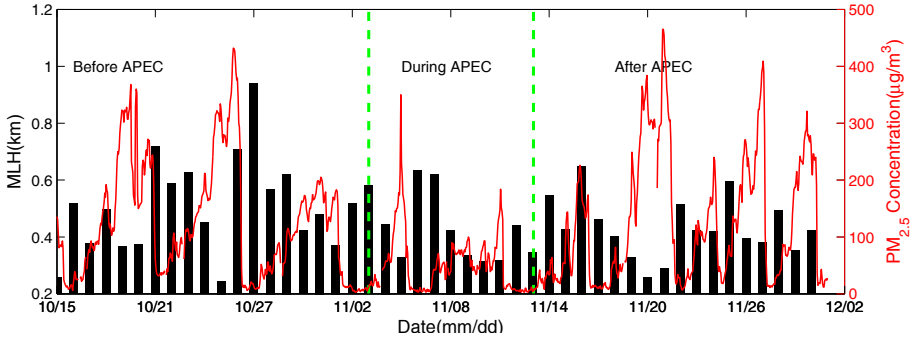

Figure 1. $PM_{2.5}$ concentrations and mixing-layer heights vs. time from 15 October to 30 November 2014.

ACPD
15, 13173–13209, 2015

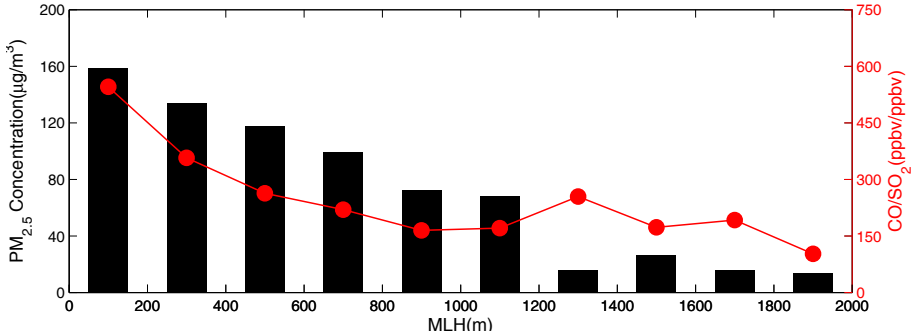

Figure 2. $PM_{2.5}$ concentrations and CO/SO_2 ratios of the mixing layer at different heights.

ACPD
15, 13173–13209, 2015

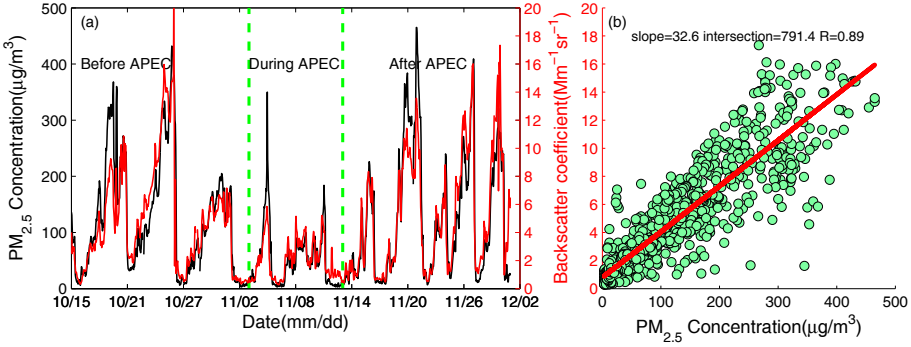

Figure 3. $PM_{2.5}$ concentrations and attenuated backscattering coefficients vs. time **(a)** and their correlations **(b)** from 15 October to 30 November 2014.

ACPD
15, 13173–13209, 2015

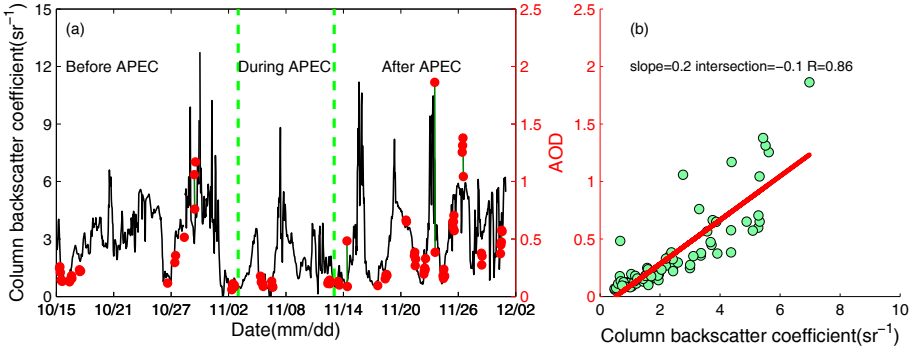

Figure 4. AOD values and 0 to 4500 m column attenuated backscattering coefficient vs. time **(a)** and their correlations **(b)**.

ACPD
15, 13173–13209, 2015

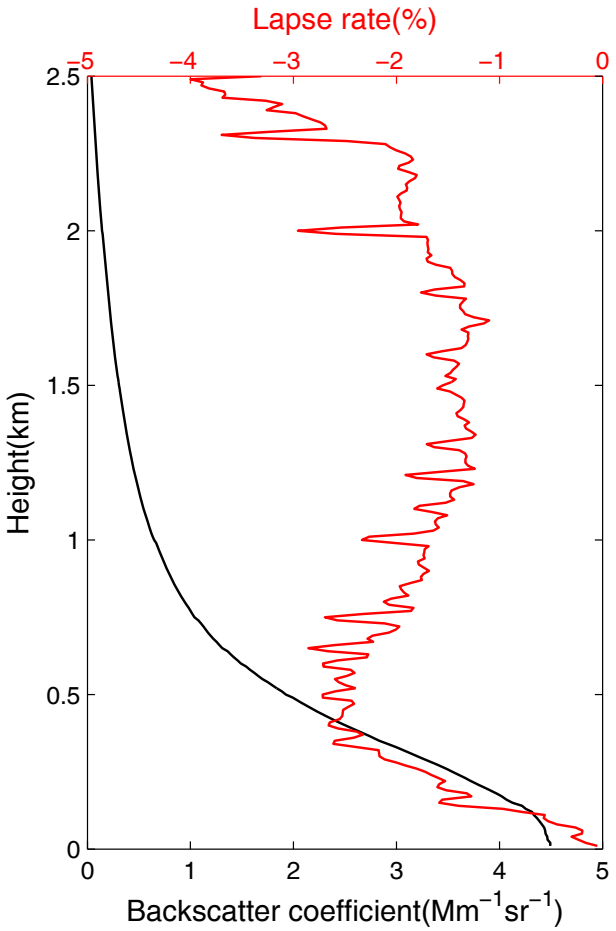

Figure 5. The attenuated backscattering coefficient vertical profiles of atmospheric aerosols and the decreasing rate.

ACPD
15, 13173–13209, 2015

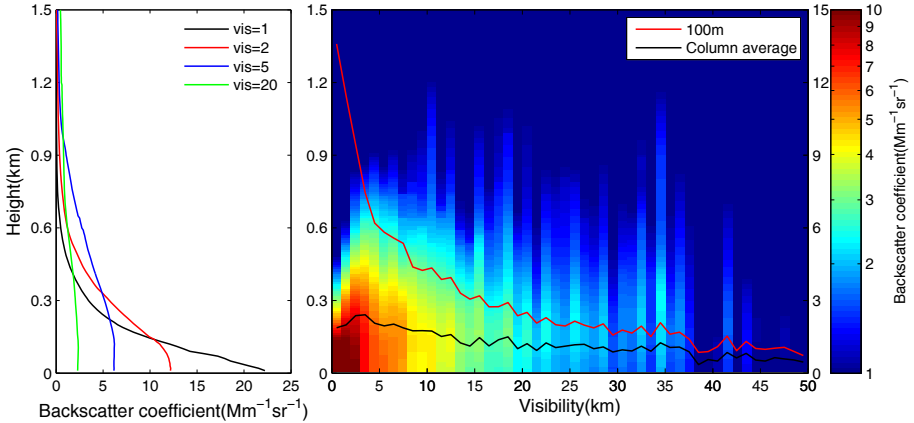

Figure 6. Variations in the vertical gradient of attenuated backscattering coefficients under different visibility conditions.

ACPD
15, 13173–13209, 2015

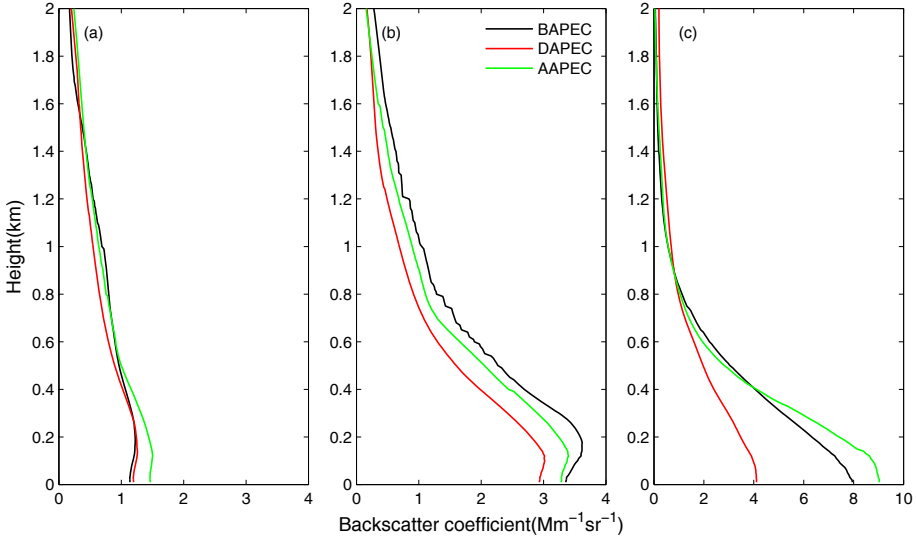

Figure 7. Backscattering profiles under different pollution conditions during the periods of BAPEC, DAPEC and APPEC **(a)** PM < 50 μg m^{-3}, **(b)** 50 μg m^{-3} < PM < 100 μg m^{-3}, **(c)** PM > 100 μg m^{-3}.

ACPD
15, 13173–13209, 2015

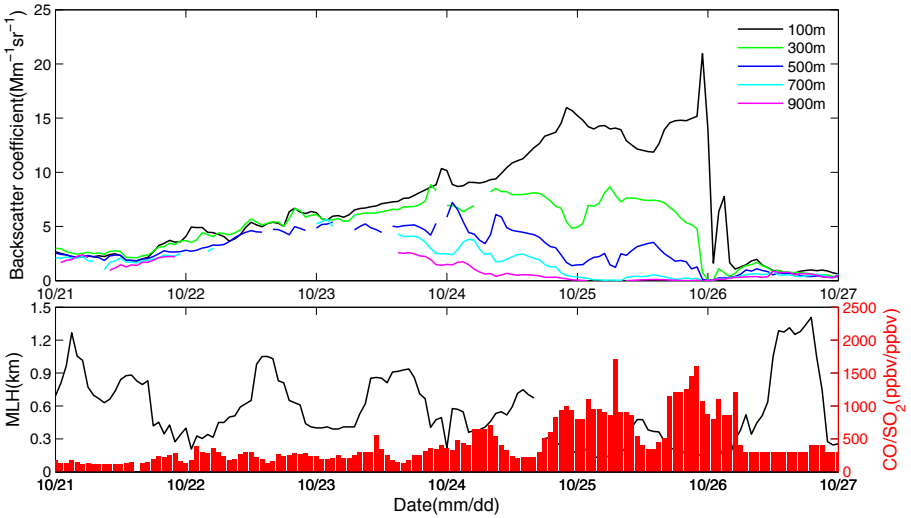

Figure 8. Variations in the attenuated backscattering coefficients at different heights and near-surface CO/SO_2 ratios from 21–26 October.

ACPD
15, 13173–13209, 2015

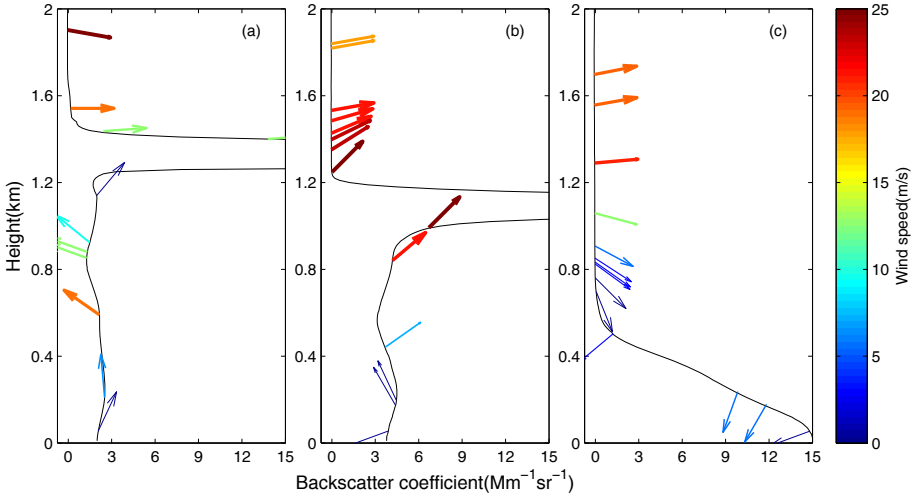

Figure 9. Attenuated backscattering coefficient profiles and wind profiles during the heavy pollution for the periods 21–26 October at **(a)** 08:00 LT on 21 October, **(b)** 08:00 LT on 22 October, and **(c)** 08:00 LT on 25 October.

ACPD
15, 13173–13209, 2015

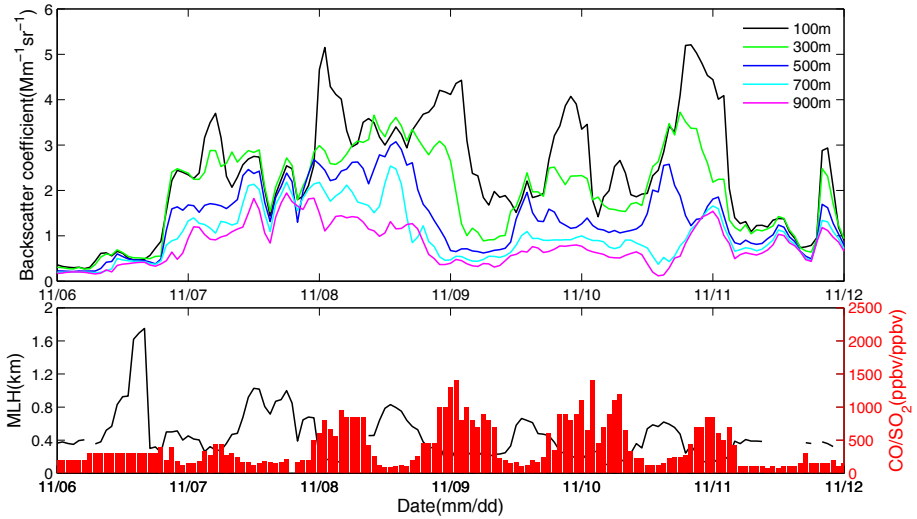

Figure 10. Attenuated backscattering coefficients at different heights and near-surface CO/SO_2 ratios for 6–11 November.

ACPD
15, 13173–13209, 2015

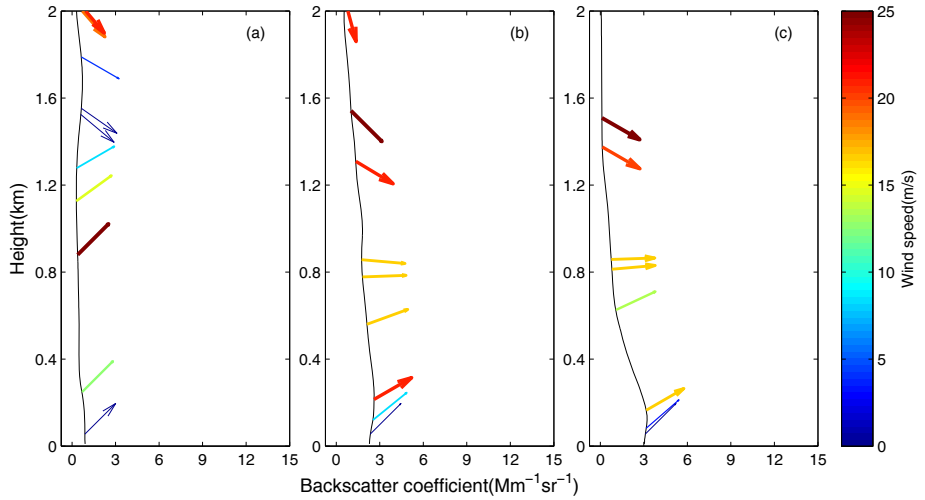

Figure 11. Attenuated backscattering coefficient profile and wind profile during the heavy pollution process for 6–11 November at **(a)** 20:00 LT on 7 November, **(b)** 20:00 LT on 8 November, and **(c)** 20:00 LT on 10 November.

ACPD
15, 13173–13209, 2015

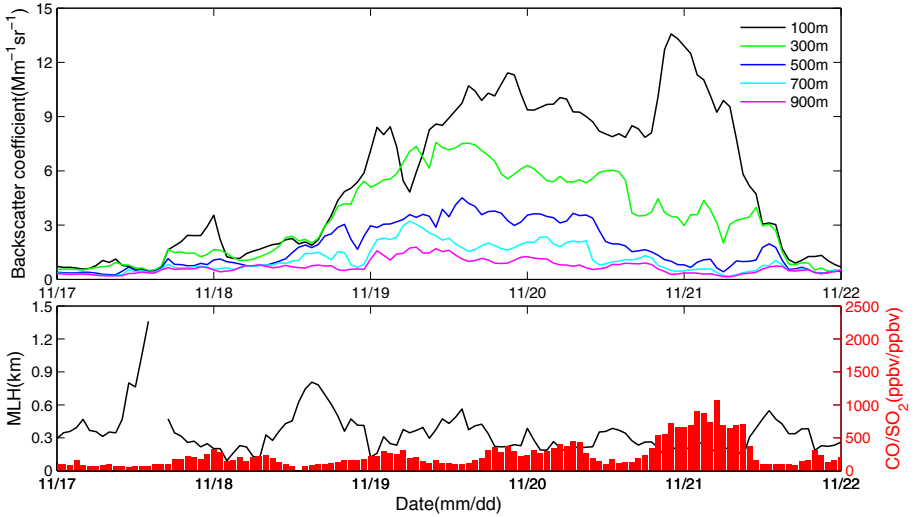

Figure 12. Attenuated backscattering coefficients at different heights and near-surface CO/SO_2 ratios for 17–21 November.

ACPD
15, 13173–13209, 2015

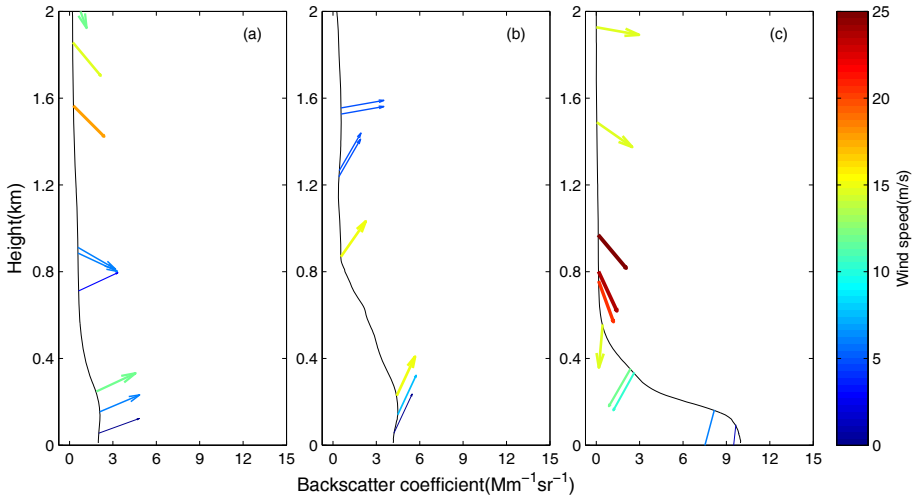

Figure 13. Attenuated backscattering coefficient profile and wind profile during the heavy pollution process for 17–21 November at **(a)** 20:00 LT on 17 November, **(b)** 20:00 LT on 18 November, **(c)** 20:00 LT on 21 November.

ACPD
15, 13173–13209, 2015